

The DarkSide-50 outer detectors

S Westerdale^c, P Agnes^a, L Agostino^b, I F M Albuquerque^{c,d},
T Alexander^{e,f}, A K Alton^g, K Arisaka^h, H O Back^{c,i}, B Baldin^f,
K Biery^f, G Bonfini^j, M Bossa^k, B Bottino^{l,m}, A Brigattiⁿ,
J Brodsky^c, F Budano^{o,p}, S Bussino^{o,p}, M Cadeddu^{q,r}, L Cadonati^e,
M Cadoni^{q,r}, F Calaprice^c, N Canci^{s,j}, A Candela^j, H Cao^c,
M Cariello^m, M Carlini^j, S Catalanotti^{t,u}, P Cavalcante^{v,j},
A Chepurinov^w, A G Cocco^u, G Covone^{t,u}, D D'Angelo^{x,n},
M D'Incecco^j, S Davini^{k,j}, S De Cecco^b, M De Deo^j,
M De Vincenzi^{o,p}, A Derbin^y, A Devoto^{q,r}, F Di Eusanio^c,
G Di Pietro^{j,n}, E Edkins^z, A Empl^s, A Fan^h, G Fiorillo^{u,t},
K Fomenko^{aa}, G Foster^{e,f}, D Franco^a, F Gabriele^j, C Galbiati^{c,j},
C Giganti^b, A M Goretti^j, F Granato^{t,bb}, L Grandi^{cc}, M Gromov^w,
M Guan^{dd}, Y Guardincerri^f, B R Hackett^z, K R Herner^f,
E V Hungerford^s, Aldo Ianni^{ee,j}, Andrea Ianni^c, I James^{o,p},
C Jollet^{ff}, K Keeter^{gg}, C L Kendziora^f, V Kobychhev^{hh}, G Koh^c,
D Korablev^{aa}, G Korga^{s,j}, A Kubankinⁱⁱ, X Li^c, M Lissia^r,
P Lombardiⁿ, S Luitz^{jj}, Y Ma^{dd}, I N Machulin^{kk,ll}, A, Mandarano^{k,j},
S M Mari^{o,p}, J Maricic^z, L Marini^{l,m}, C J Martoff^{bb}, A Meregaglia^{ff},
P D Meyers^c, T Miletic^{bb}, R Milincic^z, D Montanari^f, A Monte^e,
M Montuschi^j, M E Monzani^{jj}, P Mosteiro^c, B J Mount^{gg},
V N Muratova^y, P Musico^m, J Napolitano^{bb}, M Orsini^j, F Ortica^{mm,nm},
L Pagani^{l,m}, M Pallavicini^{l,m}, E Pantic^{oo}, S Parmeggianoⁿ,
K Pelczar^{pp}, N Pelliccia^{mm,nm}, S Perasso^a, A Pocar^{e,c}, S Pordes^f,
D A Pugachev^{kk,ll}, H Qian^c, K Randle^e, G Ranucciⁿ, A Razeto^{j,c},
B Reinhold^z, A L Renshaw^{h,s}, A Romani^{mm,nm}, B Rossi^{u,c}, N Rossi^j,
S D Rountree^v, D Sablone^j, P Saggeseⁿ, R Saldanha^{cc}, W Sands^c,
S Sangiorgio^{qq}, C Savarese^{k,j}, E Segreto^{rr}, D A Semenov^y, E Shields^c,
P N Singh^s, M DSkorokhvatov^{kk,ll}, O Smirnov^{aa}, A Sotnikov^{aa},
C Stanford^c, Y Suvorov^{h,j,kk}, R Tartaglia^j, J Tatarowicz^{bb},
G Testera^m, A Tonazzo^a, P Trinchese^t, E V Unzhakov^y,
A Vishneva^{aa}, B Vogelaar^v, M Wada^c, S Walker^{t,u}, H Wang^h,
Y Wang^{dd,h,ss}, A W Watson^{bb}, J Wilhelmi^{bb}, M M Wojcik^{pp}, X Xiang^c,
J Xu^c, C Yang^{dd}, J Yoo^f, S Zavatarelli^m, A Zec^e, W Zhong^{dd}, C Zhu^c,
and G Zuzel^{pp}

The DarkSide Collaboration

^a APC, Université Paris Diderot, CNRS/IN2P3, CEA/Irfu, Obs de Paris, Sorbonne Paris Cité, 75205 Paris, France

^b LPNHE Paris, Université Pierre et Marie Curie, Université Paris Diderot, CNRS/IN2P3, Paris 75252, France

^c Department of Physics, Princeton University, Princeton, NJ 08544, USA

^d Instituto de Física, Universidade de São Paulo, São Paulo 05508-090, Brazil
^e Amherst Center for Fundamental Interactions and Department of Physics, University of Massachusetts, Amherst, MA 01003, USA
^f Fermi National Accelerator Laboratory, Batavia, IL 60510, USA
^g Department of Physics, Augustana University, Sioux Falls, SD 57197, USA
^h Department of Physics and Astronomy, University of California, Los Angeles, CA 90095, USA
ⁱ Pacific Northwest National Laboratory, Richland, WA 99354, USA
^j Laboratori Nazionali del Gran Sasso, Assergi AQ 67010, Italy
^k Gran Sasso Science Institute, L'Aquila 67100, Italy
^l Department of Physics, Università degli Studi, Genova 16146, Italy
^m Istituto Nazionale di Fisica Nucleare, Sezione di Genova, Genova 16146, Italy
ⁿ Istituto Nazionale di Fisica Nucleare, Sezione di Milano, Milano 20133, Italy
^o Istituto Nazionale di Fisica Nucleare, Sezione di Roma Tre, Roma 00146, Italy
^p Department of Physics and Mathematics, Università degli Studi Roma Tre, Roma 00146, Italy
^q Department of Physics, Università degli Studi, Cagliari 09042, Italy
^r Istituto Nazionale di Fisica Nucleare, Sezione di Cagliari, Cagliari 09042, Italy
^s Department of Physics, University of Houston, Houston, TX 77204, USA
^t Istituto Nazionale di Fisica Nucleare, Sezione di Napoli, Napoli 80126, Italy
^u Department of Physics, Università degli Studi Federico II, Napoli 80126, Italy
^v Department of Physics, Virginia Tech, Blacksburg, VA 24061, USA
^w Skobeltsyn Institute of Nuclear Physics, Lomonosov Moscow State University, Moscow 119991, Russia
^x Department of Physics, Università degli Studi, Milano 20133, Italy
^y St. Petersburg Nuclear Physics Institute NRC Kurchatov Institute, Gatchina 188350, Russia
^z Department of Physics and Astronomy, University of Hawai'i, Honolulu, HI 96822, HI
^{aa} Joint Institute for Nuclear Research, Dubna 141980, Russia
^{bb} Department of Physics, Temple University, Philadelphia, PA 19122, USA
^{cc} Kavli Institute, Enrico Fermi Institute and Dept. of Physics, University of Chicago, Chicago, IL 60637, USA
^{dd} Institute for High Energy Physics, Beijing 100049, China
^{ee} Laboratorio Subterráneo de Canfranc, Canfranc Estación E-22880, Spain
^{ff} IPHC,19 Université de Strasbourg, CNRS/IN2P3, Strasbourg 67037, France
^{gg} School of Natural Sciences, Black Hills State University, Spearfish, SD 57799, USA
^{hh} Institute for National Research, National Academy of Sciences of Ukraine, Kiev 03680, Ukraine
ⁱⁱ Radiation Physics Laboratory, Belgorod National Research University, Belgorod 308007, Russia
^{jj} SLAC National Accelerator Laboratory, Menlo Park, CA 94025, USA
^{kk} National Research Centre Kurchatov Institute, Moscow 123182, Russia
^{ll} National Research Nuclear University MEPhI, Moscow 115409, Russia
^{mm} Department of Chemistry, Biology and Biotechnology, Università degli Studi, Perugia 06123, Italy
ⁿⁿ Istituto Nazionale di Fisica Nucleare, Sezione di Perugia, Perugia 06123, Italy
^{oo} Department of Physics, University of California, Davis, CA 95616, USA
^{pp} Smoluchowski Institute of Physics, Jagiellonian University, Krakow 30059, Poland
^{qq} Lawrence Livermore National Laboratory, Livermore, CA 94550, USA
^{rr} Institute of Physics Gleb Wataghin Universidade Estadual de Campinas, São Paulo 13083-859, Brazil
^{ss} School of Physics, University of Chinese Academy of Sciences, Beijing 100049, China

E-mail: shawest@princeton.edu

Abstract. DarkSide-50 is a dark matter detection experiment searching for Weakly Interacting Massive Particles (WIMPs), in Gran Sasso National Laboratory. For experiments like DarkSide-50, neutrons are one of the primary backgrounds that can mimic WIMP signals.

The experiment consists of three nested detectors: a liquid argon time projection chamber surrounded by two outer detectors. The outermost detector is a 10 m by 11 m cylindrical water

Cherenkov detector with 80 PMTs, designed to provide shielding and muon vetoing.

Inside the water Cherenkov detector is the 4 m diameter spherical boron-loaded liquid scintillator veto, with a cocktail of pseudocumene, trimethyl borate, and PPO wavelength shifter, designed to provide shielding, neutron vetoing, and *in situ* measurements of the TPC backgrounds. We present design and performance details of the DarkSide-50 outer detectors.

1. Introduction

Since dark matter experiments attempting to detect Weakly Interacting Massive Particles (WIMPs) are looking for very rare events, it is crucial that these experiments have as little background as possible, in order to achieve high sensitivity. Many experiments have powerful ways of rejecting electromagnetic backgrounds. For example, in liquid argon, pulse shape discrimination can be used to very efficiently reject electron recoils.

However, nuclear recoils may leave a signal in the detector that looks identical to that expected from WIMPs. Nuclear recoils can come from surface backgrounds, in which case they can be rejected with position cuts. However, those from neutron backgrounds pose a bigger challenge.

In these proceedings, we discuss the design and performance of a highly efficient neutron veto system, and its implementation as part of the DarkSide-50 experiment.

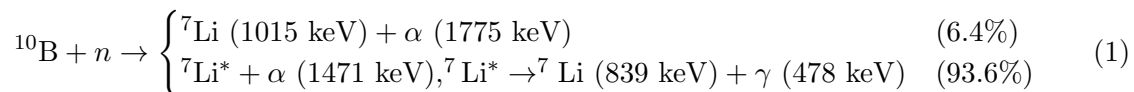
2. DarkSide-50

The DarkSide-50 detector is described in detail in [1] and [2]. It is located in Laboratori Nazionali del Gran Sasso. It consists of three nested detectors: innermost is the liquid argon time projection chamber (LAr TPC). Surrounding the LAr TPC is the liquid scintillator veto (LSV), which is inside the Water Cherenkov Veto (WCV). Together, these two outer detectors constitute the neutron veto system. The LAr TPC has an active mass of (46.4 ± 0.7) kg of liquid argon, and is currently running with underground argon, significantly reduced in the radioactive isotope ^{39}Ar . An important goal in the design of the LAr TPC was to minimize the amount of shielding that might block a neutron that scattered on the LAr from entering the LSV. This goal meant that the LAr TPC was designed to use as few low-Z materials as possible, and the neutron capture cross sections of materials used were considered as well.

The outer detectors are discussed in detail in [3]. The LSV is a 4 m diameter stainless steel sphere filled with a boron-loaded liquid scintillator viewed by 110 PMTs, and the WCV is a $10\text{ m} \times 11\text{ m}$ cylinder filled with water. The primary purpose of the WCV is to provide passive shielding to the LSV, and to detect Cherenkov light produced by muons or their electromagnetic showers, which may be associated with a cosmogenic neutron. The purpose of the LSV is to detect radiogenic neutrons that may be in coincidence with the LAr TPC, either by seeing the signal produced by the neutrons as they thermalize in the scintillator, or by detecting the thermalized neutron capture signal on ^{10}B or ^1H . Before designing these detectors in detail, GEANT4 simulations were performed to test the conceptual design of the LSV [4], and FLUKA simulations were performed to test the conceptual design of the WCV [5].

3. Neutron Capture Reactions

^{10}B was chosen as a neutron capture agent due to its high thermal neutron capture cross section of 3837 b. Neutrons may capture on ^{10}B may happen through two channels:



In the latter case, the excited state of ^7Li decays to produce a 478 keV γ -ray, which can easily be detected if it deposits its energy in the scintillator. However, if the γ -ray goes back

into the cryostat, it is possible for this signal to be lost. The short range of the α and ${}^7\text{Li}$ in both cases means that they will almost never leave the scintillator volume. However, this short range means that their scintillation light is highly quenched, so that they produce as much light as a 50–60 keV electron. This suppression means that a high light yield is needed in order to detect these reaction products, but if they can be detected, neutrons can very efficiently be vetoed.

Additionally, thermal neutrons may capture on ${}^1\text{H}$ or ${}^{12}\text{C}$ with much lower cross sections:

$$\begin{aligned}
 & {}^1\text{H} + n \rightarrow {}^2\text{H} + \gamma \text{ (2223 keV)} \quad I_\gamma/I_\gamma(\text{max}) = 100\% \quad \sigma = 0.33\text{b} \\
 & {}^{12}\text{C} + n \rightarrow \begin{cases} {}^{13}\text{C} + \gamma \text{ (3090 keV)} & I_\gamma/I_\gamma(\text{max}) = 100\% \\ {}^{13}\text{C} + \gamma \text{ (4945 keV)} & I_\gamma/I_\gamma(\text{max}) = 67\% \\ {}^{13}\text{C} + \gamma \text{ (1860 keV)} & I_\gamma/I_\gamma(\text{max}) = 57\% \end{cases} \quad \sigma = 0.0034\text{b}
 \end{aligned} \tag{2}$$

where σ is the thermal neutron capture cross section, and $I_\gamma/I_\gamma(\text{max})$ is the intensity of the γ -ray, relative to the maximum intensity γ -ray [6]. For ${}^{12}\text{C}$ only the three dominant γ -rays are shown (notably, ${}^{12}\text{C}$ will often produce multiple γ -rays after capturing a neutron).

4. Prototype Tests

While designing the LSV, a series of tests were performed using a prototype setup made from a ~ 20 L stainless steel vessel. These tests were used both to choose a reflector and scintillator cocktail combination and to ensure that this design could be used to detect neutrons. These studies are discussed in more detail in [7]. The initial tests to choose the scintillator cocktail and reflector were performed by putting 7.62 cm \times 7.62 cm cylindrical glass cells in the prototype detector, filled with different scintillator cocktails, while the inside of the prototype was lined with the reflector we were testing. Separate tests were performed to determine the compatibility of the scintillator and reflectors, in which we submerged the reflectors in a glass vessel containing the scintillator for an extended period of time; the reflector was then removed and we measured its reflectance in a spectrophotometer.

4.1. Scintillator Cocktail Choice

Due to experience gained with Borexino showing that pseudocumene (PC) can be used for a high-light yield scintillator [8], we decided to use PC as the primary scintillator. PC mixes well with trimethyl borate (TMB), the boron-loading agent, and a cocktail containing 50% PC has a scintillation yield 85% of that obtained with a pure PC sample. The wavelength shifters 2,5-diphenyloxazole (PPO) and 1-phenyl-3-mesityl-2-pyrazoline (PMP) were considered at various concentrations. However, while PMP was found to result in a higher scintillation yield, it was discarded due to availability constraints. We also considered using 1,4-Bis(2-methylstyryl) benzene (bis-MSB) or 1,4-bis(5-phenyloxazol-2-yl) benzene (POPOP) as secondary wavelength shifters, but found that they did not increase the light yield enough to warrant their use.

Finally, a cocktail containing 50% PC, 50% TMB, and 3 g/L PPO was chosen, as it was found to give a high light yield when used in conjunction with the reflector we settled on.

4.2. Reflector Choices

When choosing a reflector, it was important to consider its compatibility with PC and TMB. Many reflectors work by using void-based technology, where the different indices of refraction of the material and the voids cause the reflector to be highly reflective. However, while these reflectors are often sufficiently hydrophobic to keep water from filling the voids, we found PC may still do so and cause the reflector to become translucent. Other reflector candidates were discarded due to chemical incompatibility with PC or TMB.

We found that Lumirror 188 E6SR and Tyvek 4077D lost little reflectance when submerged in the scintillator. Lumirror has protective layers on both sides, which keep scintillator from

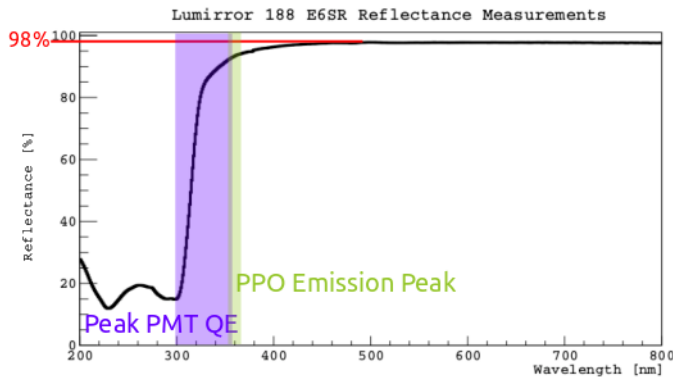


Figure 1. Lumirror 188 E6SR reflectance measurement. (Purple) The area around the PMT peak quantum efficiency. (Green) The area around the peak of the PPO emission spectrum. [7]

filling its voids. Tyvek 4077D has a protective titanium oxide coating. We found that Tyvek 4077D had a cutoff in reflectance below ~ 400 nm, while Lumirror had a cutoff below ~ 300 nm. The lower wavelength cutoff for Lumirror meant that we could get a high light yield without the use of a secondary wavelength shifter, while we would need one with Tyvek 4077D. As a result, we decided to use Lumirror in the LSV. It should be noted that while we found the bulk of the Lumirror maintained a high reflectance when submerged in PC and TMB for an extended period of time, a slow degradation was observed around the edges, where the reflectance dropped to a peak reflectance of $\sim 83\%$ at a rate of about 1 cm every nine months. This rate was slow enough that we did not expect it to be a problem for a three years of running. However, as an additional safety precaution, we overlapped the layers Lumirror by about 5 cm when we installed them in the LSV. Figure 1 shows the reflectance measured for Lumirror 188 E6SR compared to the peak quantum efficiency of the PMTs used in the LSV and the PPO emission spectrum.

Since water does not fill the voids in Tyvek like PC does, we used Tyvek 1082D to line the inner surfaces of the WCV.

4.3. Prototype Performance

We then lined the prototype with Lumirror and filled it with the scintillator. Using a ^{54}Mn γ -ray source, we measured a light yield of 0.466 ± 0.001 photoelectrons/keV (PE/keV). This light yield decreased by about $0.52 \pm 0.02\%$ /week, which we attributed to metal oxides in the stainless steel reacting with the PC. This effect should scale with the surface-to-volume ratio. We determined that this effect should be small for a 4 m diameter LSV, and that re-distillation campaigns can be performed if necessary.

Measurements taken with an $^{241}\text{AmBe}$ source showed that the $\alpha + ^7\text{Li}$ produced by the neutron capture on ^{10}B could be seen in the prototype. Optical simulations of the prototype were performed using measured values for the optical parameters of the relevant materials and agreed with the measured light yield of the prototype to within $\sim 2\%$. Scaling this simulation to the full LSV geometry planned for DarkSide-50 predicted a light yield of 0.48 PE/keV, high enough to see the neutron capture reaction products.

5. The DarkSide-50 Veto System

Once the DarkSide-50 detector systems were constructed and filled, we began taking data. Data taking campaigns can be divided into two phases, based on different scintillator cocktails used in the LSV. Both campaigns are summarized in Table 1.

The primary difference between the two campaigns is the amount of TMB used. The reason for this change was that after filling the LSV, we found an overwhelming background from ^{14}C decays. ^{14}C is present in Earth's atmosphere and β -decays with a Q-value of 156 keV and

Table 1. Summary of the two different scintillator cocktails used by the DarkSide-50 LSV.

Phase	% PC	% TMB	PPO Concentration [g/L]	^{14}C Activity	Light Yield
I	50	50	2.5	~ 200 kBq	>0.5 PE/keV
II	95	5	1.4	0.245 kBq	>0.5 PE/keV

a half-life 5700 years. We found that the supplier from which we bought our TMB derived their TMB from petroleum in their US plant and plant-based methanol in their European plant. Since plants exchange carbon with the atmosphere, plant-derived methanol tends to have approximately atmospheric levels of ^{14}C . However, since petroleum has spent millions of years underground, shielded from cosmic radiation, most of the ^{14}C has decayed away. While our initial studies used TMB from the US plant, our initial batch of TMB came from the European one. As a result, we observed a background of ~ 200 kBq of ^{14}C decays in the LSV.

After measuring the ^{14}C contamination of the TMB from the US plant using the accelerator mass spectroscopy facilities at Lawrence Livermore National Laboratory, we decided to replace the high- ^{14}C TMB with this new batch. However, due to cost and time constraints, we only filled back up to 5% TMB and 1.4 g/L PPO. Figure 2 shows the change in ^{14}C contamination.

Phase I lasted from November 2013 to June 2014. At this TMB concentration, the thermal neutron capture time was ~ 2.2 μs , and $\sim 0.8\%$ of neutrons were expected to capture on ^1H . Phase II began February 2015 and is still ongoing. During this phase, the thermal neutron capture time is ~ 22 μs , and $\sim 8\%$ of neutrons are expected to capture on ^1H .

6. LSV Performance

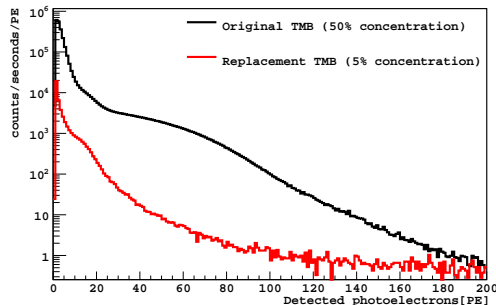


Figure 2. The low energy spectrum around the energy range of the ^{14}C β -spectrum. (Black) the spectrum during Phase I. (Red) The spectrum during Phase II. [3]

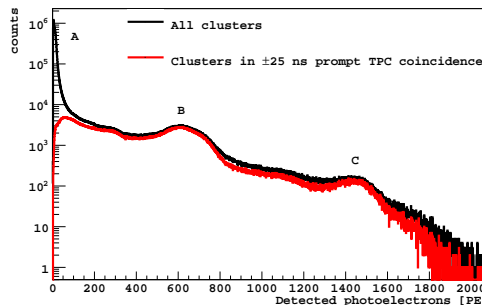


Figure 3. The energy spectrum seen by the LSV during Phase II. (Black) The distributions of all scintillation events. (Red) Those in prompt coincidence with the TPC. [3]

Figure 3 shows the energy spectrum seen by the LSV with a light yield of ~ 0.56 PE/keV during Phase II. The spectrum for all scintillation events observed shows a large spike at low energies in the region labeled A, which does not appear in the prompt coincidence spectrum. This low energy spike is largely attributed to afterpulses, though is not yet entirely understood. The region labeled B is primarily from ^{60}Co decays in the stainless steel of the TPC cryostat. Since ^{60}Co produces two γ -rays with each decay, one at 1.17 MeV and one at 1.33 MeV, it dominates much of the LSV's prompt coincidence energy spectrum, since one of these γ -rays may trigger the TPC while the other can go directly into the LSV. At higher energies, around the region labeled C, is the contribution of ^{208}Tl , which is part of the ^{232}Th decay chain. The

full energy peak of the 2.6 MeV γ -rays from ^{208}Tl is easily identified, as it is the highest energy γ -ray expected to be present in the detector, and it is often in coincidence with a 583 keV γ -ray, which may trigger the TPC while the 2.6 MeV γ -ray goes into the scintillator.

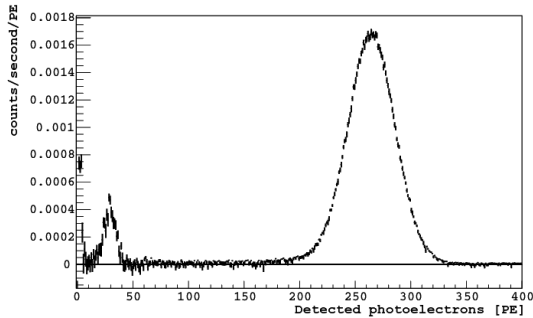


Figure 4. The neutron capture energy spectrum measured with an $^{241}\text{AmBe}$ neutron calibration source. The decay to the ^7Li excited state can be seen in the range 200–320 PE, and the decay directly to the ^7Li ground state can be seen in the range 10–40 PE. [3]

To measure the scintillator’s response to neutron captures, an $^{241}\text{AmBe}$ (α, n) neutron source was lowered into the LSV. The energy spectrum for neutron captures during Phase II can be seen in Figure 4. Between 10 and 40 PE, we can see the energy deposited by the α and ^7Li from the neutron capture on ^{10}B going directly to the ground state of ^7Li . This is well above the detection threshold of the LSV, allowing the LSV to detect neutron captures very efficiently.

7. Neutron Vetoing Efficiency

Based on the calibration data obtained so far, we estimate that the LSV can detect neutron capture signals with an efficiency $> 99.1\%$. The primary loss comes from the neutrons that capture on ^1H instead of ^{10}B , which we expect to happen for $\sim 7.7\%$ of all neutron captures. We estimate from calibration data and Monte Carlo simulations that there is a $\sim 8\%$ chance that the resultant 2.2 MeV γ -ray will go into the TPC cryostat without depositing a visible signal in the LSV, leading to a 0.62% loss of neutron captures. The next biggest comes from the $\sim 0.23\%$ of neutrons that capture after the LSV’s data acquisition window; the length of the acquisition window was chosen so that this source of inefficiency would be adequately small.

The total neutron vetoing efficiency depends on the efficiency with which the LSV can detect neutron captures and thermalization signals, as well as the probability of neutrons capturing on the TPC materials without leaving any signal in the LSV at all. Monte Carlo suggests that this third factor leads to an inefficiency of $\sim 0.05\%$. We expect the first two to be independent of each other, given that the neutron enters the LSV. The $^{241}\text{AmBe}$ calibration source produced too many γ -rays in prompt coincidence with the neutron to allow us to reliably assess the strength of the thermalization signal; a calibration campaign with a ^{241}AmC source, which is expected to have fewer high energy γ -rays, is currently underway and will make this analysis possible. In the meantime, preliminary estimates based on the quenching model presented in [9] indicate that the neutron thermalization signal will bring the total neutron vetoing efficiency above the goal of 99.5% needed to run DarkSide-50 for three years free of neutron backgrounds.

References

- [1] Agnes P, *et al.* (The DarkSide Collaboration) 2015 *Phys. Lett. B* **743** 456–466
- [2] Agnes P, *et al.* (the DarkSide Collaboration) 2015 *arXiv:1510.00702* [*astro-ph, physics:hep-ex, physics:physics*]
- [3] Agnes P, *et al.* (The DarkSide Collaboration) 2015 *arXiv:1512.07896* [*physics:ins-det*]
- [4] Wright A, Mosteiro P, Loer B, and Calaprice F P 2011 *Nucl. Inst. Meth. A* **644** 18–26
- [5] Empl A, Hungerford E V, Jasim R, and Mosteiro P 2014 *JCAP* **2014** 064–064
- [6] Chadwick M B, *et al.* 2011 *Nucl. Data Sheets* **112** 2887–2996 ISSN 0090-3752
- [7] Westerdale S, Shields E, and Calaprice F 2015 *arXiv:1509.02782* [*hep-ex, physics:physics*] ArXiv: 1509.02782
- [8] Lombardi P 2014 *Int. J. Mod. Phys. A* **29** 1442003 ISSN 0217-751X
- [9] Hong J, *et al.* 2002 *Astroparticle Physics* **16** 333–338